

Accepted Manuscript

Illustration for series of new metal ion complexes extracted from pyrazolone derivative, spectral, thermal, QSAR, DFT/B3LYP, docking and antitumor investigations

Fawaz A. Saad, Nashwa M. El-Metwaly, Thoraya A. Farghaly, Marwa G. El-Ghalban, Gamil A. Al-Hazmi, Kamel. A. Saleh, Mohammad Y. Alfaifi

PII: S0167-7322(16)33393-1
DOI: doi:[10.1016/j.molliq.2016.11.035](https://doi.org/10.1016/j.molliq.2016.11.035)
Reference: MOLLIQ 6579

To appear in: *Journal of Molecular Liquids*

Received date: 29 October 2016
Revised date: 7 November 2016
Accepted date: 9 November 2016

Please cite this article as: Fawaz A. Saad, Nashwa M. El-Metwaly, Thoraya A. Farghaly, Marwa G. El-Ghalban, Gamil A. Al-Hazmi, Kamel. A. Saleh, Mohammad Y. Alfaifi, Illustration for series of new metal ion complexes extracted from pyrazolone derivative, spectral, thermal, QSAR, DFT/B3LYP, docking and antitumor investigations, *Journal of Molecular Liquids* (2016), doi:[10.1016/j.molliq.2016.11.035](https://doi.org/10.1016/j.molliq.2016.11.035)

This is a PDF file of an unedited manuscript that has been accepted for publication. As a service to our customers we are providing this early version of the manuscript. The manuscript will undergo copyediting, typesetting, and review of the resulting proof before it is published in its final form. Please note that during the production process errors may be discovered which could affect the content, and all legal disclaimers that apply to the journal pertain.

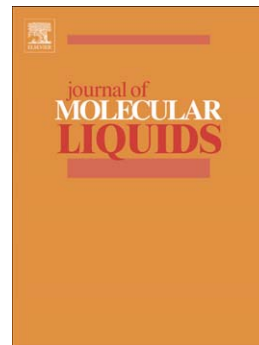


Illustration for series of new metal ion complexes extracted from pyrazolone derivative, spectral, thermal, QSAR, DFT/ B3LYP, docking and antitumor investigations

Fawaz A. saad¹, Nashwa M. El-Metwaly^{1,2*}, Thoraya A. Farghaly^{1,3}, Marwa G. El-Ghalban^{1,2}, Gamil A. Al-Hazmi^{4,5}, Kamel. A. saleh⁶, Mohammad Y. Alfaifi⁶

¹Department of Chemistry, Faculty of Applied Science, Umm Al-Qura University, Makkah Almukarramah, Saudi Arabia.

²Chemistry Department, Faculty of Science, Mansoura University, Mansoura, Egypt

³Department of Chemistry, Faculty of Science, University of Cairo, Giza, 12613, Egypt

⁴Chemistry Department, Faculty of Science, King Khalid University, P.O. Box 9004, Abha, Saudi Arabia

⁵Chemistry Department, Faculty of Applied Sciences, Taiz University, P.O. Box 82, Taiz, Yemen

⁶Biology Department, Faculty of Science, King Khalid University, P.O. Box 9004, Abha, Saudi Arabia

Abstract

New VO(II), Mn(II), Co(II), Ni(II) and Cu(II) - pyrazolone complexes were isolated and deliberately characterized. The analytical and spectral tools emphasis on the isolation of bi-nuclear complexes except Mn(II) one. Spectral parameters and reduced magnetic moments are the bases for proposing bi-nuclear complexes. Variable coordination nos. are observed with isolated complexes in-between four, five or six coordination around central atoms. TG analysis and kinetic parameters are concerned in study to examine the thermal stability of complexes. Implementing Gaussian09 program to optimize the structural formula for the investigated compounds. Applying DFT/B3LYP method, the frontier energy gapes were calculated and other important theoretical parameters. QSAR calculations proposes a distinguish biological activity for pyrazolone ligand. Molecular docking using Auto Dock tools were utilized to explain the experimental behavior of the organic compound towards the microorganisms through theoretical visualization. The docked complexes of 2YXS, 2CGY and 2JW2 protein receptors for prostate, colon and liver carcinoma were investigated and the complexation energies were calculated. The estimated energies display best expectation for excellence antitumor activity for pyrazolone compound towards variable carcinoma. IC₅₀ calculated represent an excellent priority for Cu(II) complex in overcoming liver and prostate carcinoma cell lines in comparing with reference drug. Moreover, the Mn(II) complex displays high comparative impact also with colon carcinoma.

Keywords: DFT/B3LYP, Molecular Docking, Spectral, TEM, Antitumor

* *Corresponding author:* Prof. Nashwa El-Metwaly

E mail address: n_elmetwaly00@yahoo.com

Telephone No. : +9660538553123

1. Introduction

Pyrazolone compounds refer to class of 5- membered ring structures include two nitrogen atoms and one carbonyl group. Their chemistry is significantly interesting because their extensive applications in therapeutic field [1-3] and anti-inflammatory[4]. The coordination chemistry will be enriched with the use of such important compound. The former studies introduces Zn(II) and Hg(II) metal ion complexes derived from pyrazolone derivatives with potential antitumor activity[6]. Also, in agriculture, they are used as pesticides [7]. Pyrazoles are potential appreciate to form complexes, they are suitable agents for investigating active sites of bio-molecules [8] and for modeling bio-systems for oxygen transfer [9]. Metal ions are usually bonded to the imidazole moiety of histidine, which is a part of proteins in living organisms. From the literature reports [10], both of pyrazole and imidazole are proper to mimic enzymatic reactions. The coordination chemistry of oxovanadium and copper ions are highly concerned because of their important role in biological and catalytic systems [11-13]. This is due to their electronic configuration are easily specified by EPR study. The aim of the work is the use of synthesized pyrazolone derivative includes multi-donor centers to give a great chance for poly-nuclear complexes. Such poly-nuclear complexes will serve Excellency in the biological field based on the intensive effect of the metallic role and pyrazolone ring. All possible spectral and analytical tools will be used to inspect the structural formula of the complexes. Computational studies will be utilized to deepen the study, Gaussian09 molecular modeling, QSAR and Autodock tools. Antitumor activity will be concerned against three carcinoma cell lines to give a clear insight about the expected biological efficiency for the poly-nuclear complexes in comparing with original ligand and referenced drug.

2. Experimental

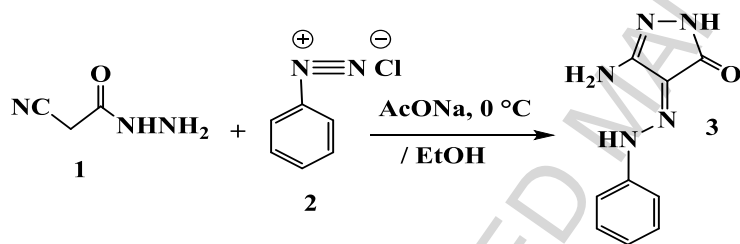
2.1. Reagents

The chemicals used in this study to prepare pyrazolone ligand; cyanoacetic hydrazide, sodium acetate tri-hydrate and sodium nitrite were purchased from Fulka and employed as it is. The metal salts used for complexation are $\text{VO}_2\text{SO}_4 \cdot \text{XH}_2\text{O}$, $\text{MnCl}_2 \cdot 4\text{H}_2\text{O}$, $\text{CoCl}_2(\text{H}_2\text{O})_6$, $\text{NiCl}_2(\text{H}_2\text{O})_6$ and $\text{CuCl}_2 \cdot 2\text{H}_2\text{O}$, were commercially available from Sigma-Aldrich. The solvents used in synthesis process are utilized without previous purification.

2.2. Synthesis

2.2.1. Synthesis of (Z)-3-amino-4-(2-phenylhydrazono)-1-H-pyrazol-5(4H)-one

Pyrazolone derivative was prepared as reported previously [14]. Freshly prepared cyanoacetic hydrazide (0.99g, 0.01 mol) in ethanol (50 ml) was stirred with sodium acetate trihydrate (1.36 g, 0.01 mol) for 15 min. The mixture was put in ice bath to 0-5 °C. While, the solution was cooled, arenediazonium chloride was prepared by diazotizing the appropriate aniline derivative (0.01 mol) in 6 M hydrochloric acid (6 mL) with cold sodium nitrite solution (10 ml, 1M) as usual. Diazonium salt solution was added drop wisely (20 min.) to a cold solution of cyanoacetic hydrazide. While stirring and keeping the temperature below 5°C, the resulting mixture was left for 3 h in a refrigerator. The synthesized arylhydrazone was filtered off and exsiccated. Refluxing of ethanolic arylhydrazone for 2hr gives, 3-amino-4-(2phenylhydrazono)-4,5-dihydropyrazol-5-ones (HL) ligand [scheme 1].



Scheme 1. Synthesis of pyrazolone ligand (HL)

2.2.2. Synthesis of metal ion complexes

Synthesis process was implemented at normal conditions of mixtures pHs. Equi-molar ratios (1 : 1) were mixed from pyrazolone ligand (HL) to each metal salt. 1.016g (5 mmol) of pyrazolone ligand was dissolved in ethanol. Then, added drop wisely to each metal salt solution attributed to, $\text{VOSO}_4 \cdot \text{XH}_2\text{O}$ (0.815g), $\text{MnCl}_2 \cdot 4\text{H}_2\text{O}$ (0.990g), $\text{CoCl}_2(\text{H}_2\text{O})_6$ (1.190g); $\text{NiCl}_2(\text{H}_2\text{O})_6$ (1.190g) and $\text{CuCl}_2 \cdot 2\text{H}_2\text{O}$ (0.853g). The mixtures refluxed for 3 – 4 h, the colored precipitates were filtered off washed with ethanol, Et_2O and finally dried in a vacuum desiccators. The influence of ligand charge transfer character is clearly affecting on colors of complexes.

2.3. Cytotoxicity against tumor cells

The toxicity of isolated complexes as well as their original salts were tested against HCT-116, HEPG-2 and PC-3 tumor cell lines by sulfo-rhodamine B (SRB). Cells were preserved in RPMI media appended with streptomycin (100 $\mu\text{g}/\text{mL}$), penicillin (100 units/mL) and 10% heat-inactivated fetal bovine serum in a humidified, 5% (v/v) carbon dioxide atmosphere at 37 °C, the cells were sub-cultured tow times in a week. Exponentially resurgent cells were collected using 0.25% tryps in-EDTA and plated in 96-wellplates at 1000cells/well. Cells were exposed to the

extracts for 72h and subsequently fixed with TCA (10%) for 1h at 4°C. After cells were washed several times, they were exposed to 0.4% SRB solution for 10 min in a dark place and then washed with 1% AcOH. After drying over night, Tris–HCl was used to dissolve the SRB-stained cells and the color intensity was measured at 540 nm. The cell viability was measured by Trypan blue (0.4) stain, permit us to distinguish viable (non-stained) and dead (stained) cells from each other. Viable and dead cells were counted with Nikon microscope with the assistance of hemocytometer. Viable cell percentage = $[1.00 - (\text{Number of blue cells} \div \text{Number of total cells})] \times 100$. The statistical analysis was accomplished through the use of Sigma Plot version 12.0

2.4. Equipments

Carbon, H and N were analyzed at Micro analytical unit. The content of metal and the conjugated anions were estimated by utilizing standard methods [15]. The infrared spectra, as KBr discs, were recorded on JASCO FT-IR-4100 Spectrophotometer ($400\text{--}4000\text{cm}^{-1}$). The electronic and ^1H NMR (200 MHz) spectra were recorded on UV₂ Unicam UV/Vis, and a Varian Gemini Spectrophotometers. The effective magnetic moments were estimated at the ordinary temperature by applying $\mu_{\text{eff}} = 2.828 \sqrt{X_M T}$, where X_M is the molar susceptibility corrected using Pascal's constants for diamagnetism of all atoms in the ligand using a Johnson Matthey magnetic susceptibility balance. Thermal analysis was carried out on a Shimadzu thermogravimetric analyzer at a heating rate of $10^\circ\text{C min}^{-1}$ under nitrogen. X-ray diffraction types (XRD) were acquired on Pikagu diffractometer by utilizing Cu / $K\alpha$ radiation. Scanning electron microscopy (SEM) images were possessed in Joel JSM-6390 tools. ESR spectra of VO(II) and Cu(II) powdered complexes were obtained on a Bruker EMX Spectrometer working in the X-band (9.60 GHz) with 100 kHz modulation frequency. The microwave power was set at 1 mW, and modulation amplitude was set at 4 Gauss. The low field signal was obtained after 4 scans with a 10 fold increase in the receiver gain. A powder spectrum was obtained in a 2 mm quartz capillary at ordinary temperature.

2.5. Theoretical calculations

2.5.1. Kinetic studies

All the kinetic parameters assigned to thermal analysis were abstracted from TG curves and tabulated. The order (n) and the energy of activation (E) were determined for suitable decomposition stages. Formerly, different researchers [16-24] were established equations and

discussing their advantages. The rate of decomposition is the product of two separate functions of temperature and conversion using:

$$\frac{d\alpha}{dt} = k(T)f(\alpha) \quad (1)$$

where, α is the fraction decomposed at time t , $k(T)$ is the temperature dependent function and $f(\alpha)$ is the conversion function. The rate constant and dependent function $k(T)$ is of Arrhenius type.

$$K = A e^{-E^*/RT} \quad (2)$$

where R , is the gas constant in ($J \text{ mol}^{-1} \text{ K}^{-1}$) substituting equation (2) into equation (1) we get this equation :

$$\frac{d\alpha}{dT} = \left(\frac{A}{\varphi e^{-E^*/RT}} \right) f(\alpha) \quad (3)$$

where φ , is the linear heating rate (dT/dt). From the integration and approximation, this equation can be obtained in the following form:

$$\ln g(\alpha) = \frac{-E^*}{RT} + \ln \left[\frac{AR}{\varphi E^*} \right] \quad (4)$$

where $g(\alpha)$ is a function depends on the mechanism of reaction. The right hand side is known as temperature integral and has no close for solution. So, several techniques have been used to evaluate the temperature integral. The kinetic parameters for the ligand and its complexes are evaluated using Coat-Redfern [18] and Horowitz-Metzger methods [23].

2.5.2. Molecular modeling methodology

The optimized structural geometry of pyrazolone and its complexes were executed by DFT/B3LYP method with different base sets using Gaussian09 software [25]. Gauss-View molecular visualization program are used to display Gaussian files [26]. In agreement with the numerical pattern appeared in the view of the compounds in gas phase, DFT/B3LYP quantum chemical parameters are calculated from HOMO–LUMO energies. Also, significant bond lengths, oscillator strength, excitation energy and effective charges for coordinating groups in optimized structures will be deducted. QSAR computations were performed for the ligand to expect its biological activity.

2.5.3. Molecular docking

Implementing Autodock tools 4.2, docking computations applying Gasteiger partial charges added to ligand (designed drug) atoms, were executed. On the ligand- protein pattern, the calculations were executed. Non-polar hydrogen atoms were conjoined, and rotatable bonds were clarified. After

the addition of; fundamental hydrogen atoms, Kollman united atom type charges and salvation parameters the Auto Dock tools were applied [27]. Autogrid program were used to accomplish affinity (grid) maps of $\times\times$ Å grid points and 0.375 Å spacing [28]. Determining Vander Waals and electrostatic terms were performed by Auto Dock parameter set- and distance-dependent dielectric functions, respectively. Simulative docking were executed by Solis & Wets local search method and Lamarckian genetic algorithm (LGA) [29]. Incidentally, initial position, orientation and torsions of ligand molecule were set. All rotatable torsions were emitted during docking. 10 different runs were used to derive each docking experiment, that were set to block after a ultimate of 250000 energy estimations. The size was established to 150. Throughout the study, a translational step of 0.2 Å, quaternion and torsion steps of 5 were utilized.

3. Results and discussion

3.1. General

Essential physical and analytical data for pyrazolone and its VO(II), Mn(II), Co(II), Ni(II) and Cu(II) complexes are displayed in Table 1. All the investigated complexes have high melting points, insoluble in all organic solvents except DMSO and DMF are sparingly soluble. 2:1 (M:L) molar ratio is the universal formularization proposed for all investigated complexes except Mn(II) complex displays 1:1 ratio. The divergence of Mn(II) ratio may refer to its relative big size which may instable the bi-nuclear complex. Whereas, the VO(II) complex is different due to the trans effect of V=O bond which facilitates the poly-nuclear formation. The molar conductivity measurements cannot be performed due to sparingly soluble feature of the complexes which mainly attached with neutral coordination spheres. This is anticipated behavior with chloride and sulphate anions which favor their covalent attachments with metal ions.

3.2. IR and ¹H NMR

Essential vibrations of pyrazolone and its complexes were presented in Table 2. Free pyrazolone spectrum represents the following bands: 3410, 3333; 3185; 1671; 1586; 1625; 1442,1493 attributing to ν NH₂; ν NH; ν C=O; ν C=N; δ NH₂; δ NHs [30]. Its ¹H NMR (DMSO-d₆) spectrum (Fig. 1S) displays: 5.8 (s, 2H, NH₂), 7.1-7.53 (m, 6H, NH, Ar-H), 10.53 (s, 1H, NH). Its MS m/z (%) 204 (M⁺+1, 12), 203 (M⁺, 100), 126 (67), 93 (38), 77 (60), 65 (61). These varification tools introducing the best structural formual of the free organic compound which beeing confirmed with molecular modeling implementation.

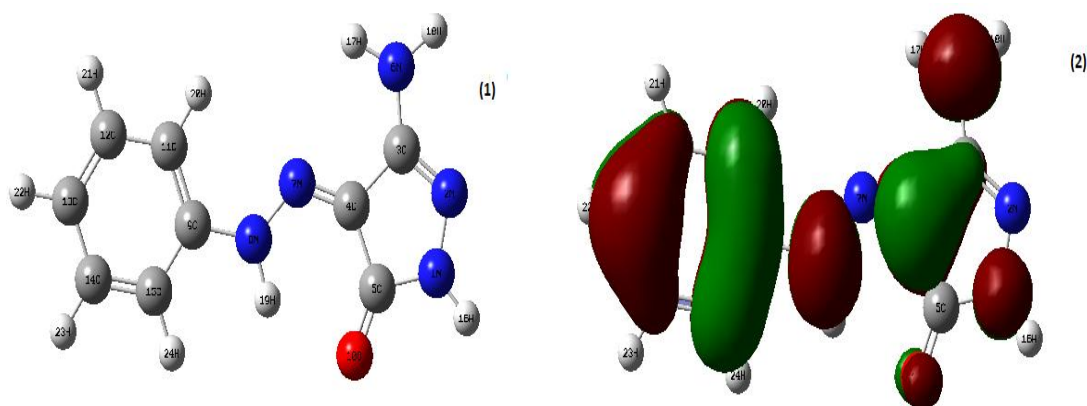


Fig. 1. Optimized and occupied geometries of pyrazolone ligand (HL)(1 and 2, respectively)

The coordination manner across central atoms was proposed from IR spectral data. Neutral tetradentate mode was suggested with bi-nuclear complexes whereas, bi-dentate mode with mono-nuclear Mn(II) one. Neutral mode appeared, reflects the relative acidity of complexation media yielded from using acidic salts for transition metals. The lower shift observed generally with νNH_2 ; νNH ; $\nu\text{C}=\text{O}$; $\nu\text{C}=\text{N}$; δNH_2 ; δNH bands in VO(II), Co(II), Ni(II) and Cu(II) complexes, verifies the coordination manner suggested by NNNO donors. While, the lower shift for $\nu\text{C}=\text{O}$; νNH and δNH bands in Mn(II) complex spectrum represents NO as coordinating sites. An observable broadness with bands assigned for νNHs and $\nu\text{C}=\text{N}$ prohibits the exact determination for non-coordinating twins groups. VO(II) complex spectrum displays new bands at 1387.7, 1319.98 and 968.8 cm^{-1} attributing to $\nu_{\text{as}}(\text{SO}_4)$, $\nu_{\text{s}}(\text{SO}_4)$ and $\nu(\text{V}=\text{O})$ vibrations. The broadness appeared at the upper region may suggest of crystal or coordinating hydrating molecules accompanied with the synthesized complexes[31]. Also, the presence of new bands assign for $\delta\text{r}(\text{H}_2\text{O})$ and $\delta\text{w}(\text{H}_2\text{O})$ vibrations [32] verifies their presence in coordinating or crystal forms. New weak bands abstracted are attributing to $\nu\text{M}-\text{N}$ and $\nu\text{M}-\text{O}$ vibrations to verify the bonding manner. $\nu\text{M}-\text{Cl}$ vibration band cannot easily detected in the scan range applied by the used IR equipment.

3.3. Electronic spectra and magnetic measurements

In DMSO solvent, significant electronic transition bands recorded for 0.1 mmol/L as well as some spectral data were recorded and tabulated(Table 3). Intra-ligand transition bands are: 31,250; 25,000 and 23,809 cm^{-1} assign for $\pi \rightarrow \pi^*$ and $\text{n} \rightarrow \pi^*$ transitions, respectively. The molar absorptivity value for $\text{n} \rightarrow \pi^*$ transition band is $\epsilon_1 = 454 \text{ mol}^{-1}\text{dm}^3\text{cm}^{-1}$ suitable for first excitation process inside pyrazolone. A moderate conjugation observed for chromophor groups in the

pyrazolone may affect on charge transfer (CT) position which close to visible region and deepen the compound color. The molar absorptivity value was elevated with the complexes first transition bands. This may refer to d-d transitions which have high oscillator strength values especially for the introductory transition step inside splitting d orbital's. $[(VO)_2(SO_4)_2(C_9H_9N_5O)] \cdot 2H_2O$ complex spectrum shows a significant band at $13,150 \text{ cm}^{-1}$ assigns for ${}^2B_2 \rightarrow {}^2E$ transition while, ${}^2B_2 \rightarrow {}^2B_1$ transition is strongly occluded with CT band at $26,521 \text{ cm}^{-1}$ in square-pyramidal configuration (Fig.2A) [33]. The reduced magnetic moment value (1.34BM) is supporting a strong interaction inside the bi-nuclear complex. $[MnCl_2(C_9H_9N_5O) \cdot 2(H_2O)]$ complex spectrum shows bands at: 18,420; 23,529; 27,027 and $31,250 \text{ cm}^{-1}$. The bands are corresponding to ${}^6A_1g \rightarrow {}^4T_1g(G^4)$, ${}^6A_1g \rightarrow {}^4Eg, {}^4A_1g(G^4)(10B+5C)$, ${}^6A_1g \rightarrow {}^4Eg, (D^4)(17B+5C)$, ${}^6A_1g \rightarrow {}^4T_1g(P^4)$ ($7B+7C$) transitions, respectively in octahedral configuration (Fig. 2B). The magnetic moment value (5.96BM) is within the normal range of high spin low field mono-nuclear d^5 complexes. The $10Dq$, Racah and nephelauxetic parameters values (8442.5 cm^{-1} , 767.5 cm^{-1} and 0.892) were calculated and displaying a soft shift from elemental shape and a significant ionic attachment may be proposed based on the β value near the upper limit ($\beta=1$) for pure ionic interaction. $[Co_2Cl_4(C_9H_9N_5O) \cdot 4(H_2O)]$ complex spectrum shows d-d transition bands at: 16,255 and $19,560 \text{ cm}^{-1}$ correspond to ${}^4T_1g \rightarrow {}^4A_2g(\nu_2)$ and ${}^4T_1g \rightarrow {}^4T_1g(p)(\nu_3)$ transitions, respectively. The calculated spectral parameter values; 8704.9 cm^{-1} , 870.5 cm^{-1} and 0.896 attributing to $10Dq$, B and β , respectively are within the range for octahedral configuration (Fig. 2C)[34]. The high β value (0.896) indicates a strong ionic interaction around metal centers [35]. The reduced magnetic moment value (4.31BM) indicates a strong metal-metal interaction inside the bi-nuclear complex. $[Ni_2Cl_4(C_9H_9N_5O)] \cdot 2H_2O$ complex spectrum shows bands at $19,450$ and $20,833 \text{ cm}^{-1}$ correspond to ${}^1A_1g \rightarrow {}^1A_2g(\nu_1)$ and ${}^1A_1g \rightarrow {}^1B_1g(\nu_2)$, transitions, respectively[36,37] in square-planar configuration. The diamagnetic appearance of the complex goes attached with square planar of d^8 systems. $[Cu_2Cl_4(C_9H_9N_5O)] \cdot 2H_2O$ complex spectrum shows a significant d-d transition band at $18,590 \text{ cm}^{-1}$ corresponds to ${}^2B_1g \rightarrow {}^2Eg$ in square-planar configuration [38]. Also, band at $20,000 \text{ cm}^{-1}$ is attributing to LMCT. The reduced magnetic moment value (1.46BM) is also an indicative for bi-nuclear complex. Generally, Intra-ligand transition bands, $n \rightarrow \pi^*$ and $\pi \rightarrow \pi^*$ expose to little shifted appearance in all complexes spectra. Changing Z and q values for 3d transition metal complexes, the inter-electronic repulsion parameter (Racah) values are varied. Whereas, Z is the functional charge of cation and q is the filling up number of d^q shell. The Racah parameter is well- expressed by the relation: $B (\text{cm}^{-1}) = 384 + 58q + 124(z+1) - 540/(z+1)$. The calculated value of manganese

ion is +1.498 and for cobalt ion is +1.436, they are considerably below than the formal oxidation states(II) this reduction is suitable for M-N or M-O bonds [39].

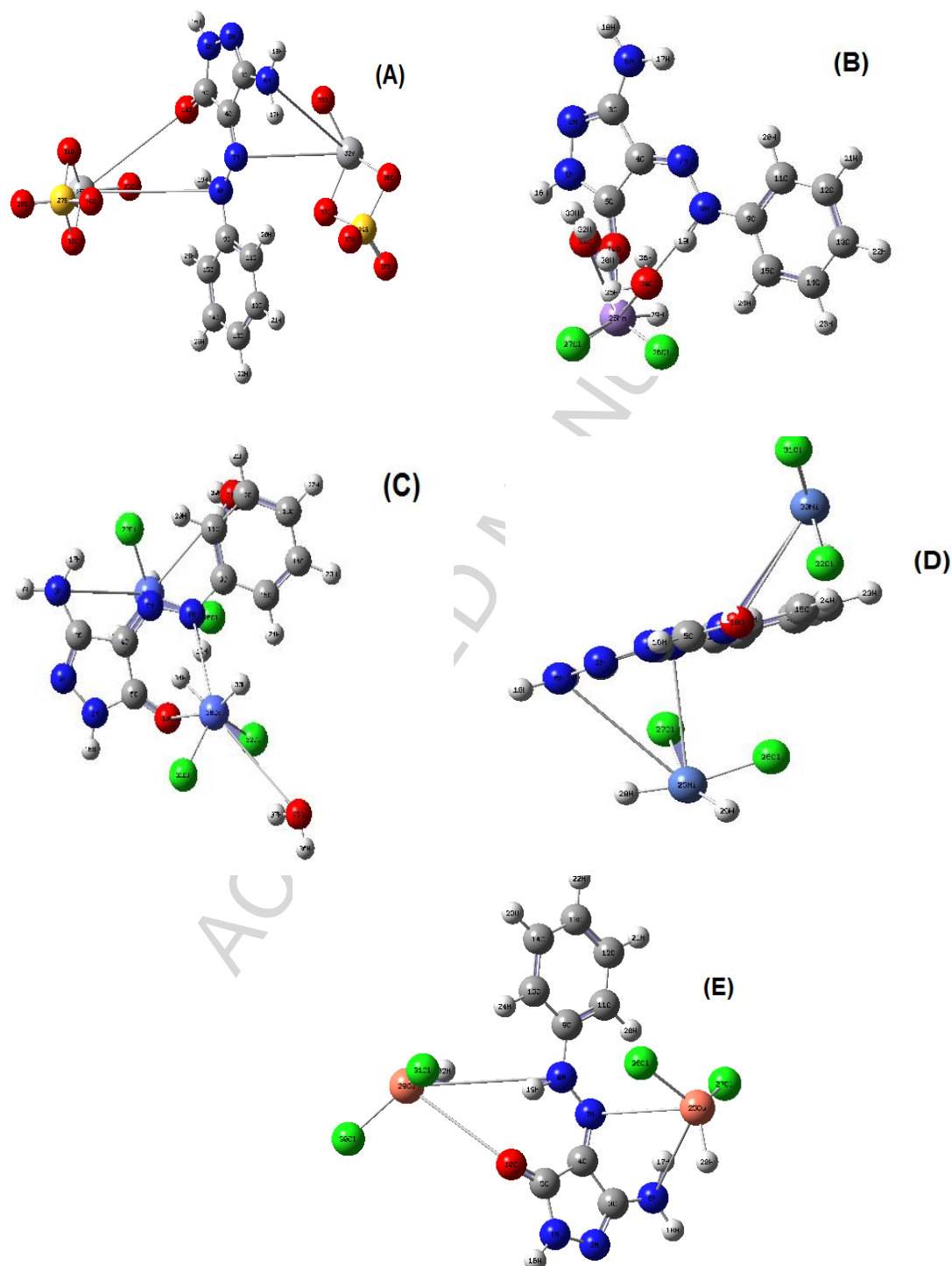


Fig. 2. The optimized geometries for, VO(II), Mn(II), Co(II), Ni(II) and Cu(II) complexes (A,B,C,D and E, respectively)

3.4. ESR spectral analysis

Spin Hamiltonian operators and the G values of solid Cu(II) and VO(II) complexes are calculated (Table 4) from their ESR spectra (Fig. 2S). The axially symmetric g tensor parameters are $g_{11} > g_{\perp} > 2.0023$ indicating that the $d_{x^2-y^2}$ orbital is a ground state [40]. The G - factor is expressed by, $G = (g_{11} - 2.0023) / (g_{\perp} - 2.0023) = 4$, which measures the exchange interaction inside the complex. According to Hathaway [41], $G > 4$, negligible exchange interaction between copper(II) centers, while, $G < 4$, is vice versa. Here, the highly reduced value(1.825) introduces a strong interaction between neighbor copper centers which express their presence inside one sphere [42,43]. This agrees with determined magnetic moment. The $g_{11}(2.336)$ value is matched with highly covalent O-M and N-M bonds [44]. The tendency of A_{11} to decrease with increasing g_{11} is an index for tetrahedral distortion ($f = g_{11}/A_{11}$) [45,46]. Whenever, the calculated value is presented in the range for square-planar configuration. The σ^2 (covalence of in-plane σ -bonding) and β^2 (covalence of in plane π -bonding) were accomplished by using: $\alpha^2 = ((A_{\parallel}/0.036) + (g_{\parallel} - 2.0023) + 3/7(g_{\perp} - 2.0023) + 0.04$ and $\beta^2 = (g_{\parallel} - 2.0023) E / -8\lambda\alpha^2$, Where λ (spin- orbital coupling) = -828 cm^{-1} for free copper ion and $E (18,590 \text{ cm}^{-1})$ is the electronic transition energy. The β^2 value indicates that, in-plane π -bonding are highly ionic, while, α^2 value indicates that in-plane σ -bonding is highly covalent [47].

The spectrum of VO^{2+} complex demonstrates an eight- line manner attributing to the analogous and vertical ingredients of g- and hyperfine (hf) A- tensors. The analogous and vertical ingredients are well resolved. Nitrogen super-hyperfine splitting is not monitored in the complex, which points out that the single electron is in the d_{xy} orbital. The pattern suggests that g and A are axially symmetric in nature. The factors A and g are appeared to be in covenant with the values commonly known for vanadyl complex in square-pyramidal geometry. The molecular orbital coefficient α^2 and β^2 were executed by.

$$\beta^2 = \frac{7}{6} \left(-\frac{A_{11}}{P} + \frac{A_{\perp}}{P} + g_{11} - \frac{5}{14} g_{\perp} - \frac{9}{14} g_e \right)$$

$$\alpha^2 = \frac{2.0023 - \Delta g}{8 \beta^2 \lambda} \quad \text{where } \Delta g = (g_{\perp} - g_{\parallel}) \times 10^{-3}$$

The negative values of β^2 command to negative α^2 values. Since hyperfine conjunction disciplinarians are negative, calculations were done taking A_{11} and A_{\perp} as negative, which gave positive values of β^2 and α^2 . The calculated, α^2 and β^2 indicate the highly ionic of in - plane σ - and π - bonding. The spectrum of the complex shows band at $13,150 \text{ cm}^{-1}$ (E_2) which assigned to ${}^2B_2 \rightarrow {}^2E$, transition. Assuming pure d-orbital's by using first- and second- order perturbation theory. The parameters

attributed to transition energy are called Spin Hamiltonian and executed by the following expression: $g_{\perp} = g_e - (2\lambda/E_2)$

Where g_e is the free- electron g value (2.0023). Using E_2 value, spin orbital coupling constant (λ) is evaluated (110.62). A value for λ of 250 cm^{-1} is reported [48] for free V^{+4} ion. The high reduction in the magnitude of λ for the double bonded oxovanadium complex $(V=O)^{+2}$ is attributed to substantial π -bonding. While, the value is inside the logical borders announced. The orbital reduction factors viz., K_{\parallel} and K_{\perp} are also calculated using: ${}^2K_{\parallel} = (g_{\parallel} - 2.00277) E / 8 \lambda$ and ${}^2K_{\perp} = (g_{\perp} - 2.00277) E / 2 \lambda$. For pure σ - bonding $K_{\parallel} \approx K_{\perp} \approx -0.77$ while, ${}^2K_{\parallel} > {}^2K_{\perp}$ signifies in plane σ -bonding, with ${}^2K_{\perp} < {}^2K_{\parallel}$ accounting for out of plane π - bonding [49].

Calculation of dipole term(p),

Dipolar term of Cu(II) complex will be determined by: $P = 2 \gamma_{Cu} \beta_o \beta_N (r^{-3})$, where γ_{Cu} is the magnetic moment of copper, β_o is the Bohr magneton, β_N is the nuclear magneton and r is the distance from nucleus to outer electron shells. While, in the VO(II) complex the value can be determined by :

$$P = \frac{7(A_{11} - A_{\perp})}{6 + 3/2 (\lambda/\Delta E_1)}$$

If A_{11} is taken to be negative and A_{\perp} positive, the value of p will be more than 270 G, which is far from the expected value. Thus, the signs of both A_{11} and A_{\perp} are used as negative and are indicated in the form of isotropic hf constant (A_o). McGarvey theoretically accomplished p value as +136 G for vanadyl complexes and the value (118.28) of this complex don't deviate much from this expected value

Calculation of MO coefficients and bonding parameters

The g values observed are different from electronic value (2.0023). This assigns to spin orbit interaction of d_{xy} ground state level. The isotropic and anisotropic, g and A parameters were calculated from Eqs; $A_o = (A_{11} + 2 A_{\perp})/3$ and $g_o = (g_{11} + 2 g_{\perp})/3$. Taking A_{11} and A_{\perp} to be negative values, K expression of; $K = - (A_o / p) - (g_e - g_o)$

Thus K (Fermi – contact term) can be determined. The Fermi contact term, k , is a sense of polarization exerted by the uneven apportionment of d -electron density on the inner core s -electron.

3.5. X – Ray diffraction

The patterns of pyrazonone ligand and its VO(II), Mn(II), Co(II), Ni(II) and Cu(II) complexes were obtained at $10^{\circ} < 2\theta < 80^{\circ}$ range [Fig. 3,3S]. XRD analysis is used to give a clear insight about lattice dynamics of solid compounds. The clear patterns from peaks attributed to reactants reflect

the obscure of any reactant pollution [50]. Ligand, Mn(II) and Cu(II) complexes patterns show crystalline diffraction peaks suitable for nano-crystalline feature, while the others are in amorphous states [51,52]. The crystallinity appeared reflects the isolation of a strictly known irregular crystallizes. While, the amorphous appearance reflects the indiscriminate orientation of atoms inside 3D space. The 2θ , d values, full width at half maximum (FWHM) of main intensity peak, intensity (%) and particle size were presented in Table 5. The crystallite size was determined by using FWHM for intense peaks by Deby–Scherrer equation; $B = 0.94 \lambda / (S \cos \theta)$, where S is the crystallite size, θ is the diffraction angle, B is FWHM, $Cu/K\alpha (\lambda) = 1.5406 \text{ \AA}$. D -spacing values are the inner crystal plane which determined by Bragg equation: $n\lambda = 2d\sin(\theta)$ at $n = 1$. The calculated sizes are present excellently in nanometer range (below 35nm).

3.6. Scanning electron microscopy

SEM was used to study the habit and the surface morphology of all investigated compounds (Fig. 4S). The images of highly magnetic compounds are not strictly resolved may be due to insufficient electron beam used to provide required resolution. Also, the micrographs are elongated rod-like and needle-shaped with numerous territorial patches. So the accurate determination for the particle sizes is completely absent [53-55]. It is obvious from this study that all the complexes crystals, were grown up from just a single molecule to several accumulated distribution with particle sizes starting from few nanometers to multi- hundred. The isolation of extended rod like crystals may happen by two nucleation process by distribution and piling up of layers growth. It is suggested that if rate of growth is faster along C -axis and a great number of growth nuclei maintain active across C -axis in comparison with vertical to C -axis, extended crystals result [56]. Habit exhibited by different crystals is slightly due to the growth along the strength bond due to anisotropy included in crystal structure bonding. When the fullness overrides a definite limit, the abnormal growth in the needles, rods and platelets is the normal result. It is reasonable to believe that the environmental conditions do change in nature and variable features of morphologies. These shapes may reflect their excellent property and thermal stability with mild catalytic activity. The spherical micrographs are observed with VO(II) and Cu(II) complexes by size ranges of: 0.11-0.34 and 0.15-0.64 μm , respectively. Generally, the micrographs indicate that the isolation of strict-defined crystals free from any impact for metal ions on external surface.

3.7. Thermal analysis

The distractive feature of the investigated compounds was translated to data displayed in Table 6. The compounds display instability towards the TG analysis except Co(II) complex. This behavior is mainly attached with the existence of occluded water molecules with metal ion complexes. Two to three endothermic degradation steps are sufficient to degrade them completely till 600-820 °C. The residual parts of complexes are mainly metal oxide completely pure from carbons. The limited degradation steps are mainly associated with polymeric structures which may expel a bulky molecule in a step. This behavior may expected with most investigated complexes. The high conformity between calculated and found weight losses is referring to exact frontier barriers of each degradation steps.

3.8. Theoretical calculations

3.8.1. Kinetic studies

In order to clarify the influence of occluded metal ions with the organic compounds on the thermal behavior, the order n and the heat of activation E for defiant degradation steps were determined using TG and DTG.

3.8.1.1 Coats – Redfern equation

The equation is an integral method, represented as :

$$\int_0^{\alpha} \frac{d\alpha}{(1-\alpha)^n} = \frac{A}{\varphi} \int_{T_1}^{T_2} \exp\left(\frac{-E^*}{RT}\right) dt \quad (5)$$

For convenience of integration initial limit T_1 , is usually taken as zero. This equation on integration gives :

$$\ln\left[\frac{-\ln(1-\alpha)}{T^2}\right] = \ln\left(\frac{AR}{\varphi E^*}\right) - \frac{E^*}{RT} \quad (6)$$

A plot of $\ln\left[\frac{-\ln(1-\alpha)}{T^2}\right]$ (LHS) versus $1/T$, E^* is the energy of activation in Jmol^{-1} extracted from

the slop and A is (S^{-1}) from the value of intercept (Fig. 5S). The activation entropy (ΔS^*) in ($\text{J K}^{-1}\text{mol}^{-1}$) was executed by:

$$\Delta S^* = R \ln\left(\frac{Ah}{K_B T_s}\right) \quad (7)$$

Where k_B is the Boltzmann constant, h is the Plank's constant and T_s is the DTG peak temperature [18]

3.8.1.2. Horowitz – Metzger equation

Using derived relation [28] i:

$$\ln[-\ln(1-\alpha)] = \frac{E}{RT_m} \Theta \quad (8)$$

Where α , is the fraction decomposed at time t and $\Theta = T - T_m$.

Plot, $\ln[-\ln(1-\alpha)]$ versus Θ (Fig. 5S), is a linear relation, the slope of which E , is evaluated and Z can be extracted from the relation :

$$Z = \frac{E\varphi}{RT_m^2} \exp\left(\frac{E}{RT_m}\right) \quad (9)$$

Where φ is rate of heating, n, is the reaction order which can be determined from:

$$n = 33.64758 - 182.295\alpha_m + 435.9073\alpha_m^2 - 551.157\alpha_m^3 + 357.3703\alpha_m^4 - 93.4828\alpha_m^5 \quad (10)$$

Where α_m is the fraction of the substance decomposed at T_m .

Enthalpy of activation ΔH^* and Gibbs free energy (ΔG^*) were deduced from $\Delta H^* = E^* - RT$ and $\Delta G^* = \Delta H^* - T\Delta S^*$, equations. The entropy of activation (ΔS^*) was abstracted by conducting equation 7 and the data were displayed in table 7. The following significant observations were listed: (i) the activation energy values are reduced (E) which may reflect the soft elongated bonds inside the coordination sphere (ii) Negative ΔS^* values may reflect the ordered state of fragments which exceeded across the degradation process. (iii) The endothermic decomposition behavior was reflected on the positive ΔH^* values. (iv) The positive ΔG^* values represent that the decomposition free energy for residue is higher than that of initial compound and non-spontaneous. The upraising of $T\Delta S^*$ values (by negative singe) than the ligand lead to override ΔG^* values due to the lower decomposition rate for the complexes [57,58]

3.8.2. Molecular modeling study

Molecular modeling theoretical tool implementing Gaussian09 program was employed for pyrazolone ligand and its metal ion complexes to abstract essential quantum parameters and optimized geometries. The border orbital energy gap between E_{HOMO} & E_{LUMO} is an essential parameter used to recognize the electronic structure of molecules and also to define their relativities [59]. MO's images of free pyrazolone (Fig. 4A,B), an observable presence of HOMO and LUMO mainly centered on donor atoms, nitrogen's and carbonyl oxygen, which are considered the location for donors and acceptors. MO's images of metal ion complexes display an observable location for HOMO and LUMO levels with donor sites beside Mn(II) and Co(II) centers. while, the ruling out of

VO(II), Ni(II) Cu(II) centers, which may reflect the flexibility of charge transfer with big sizes central atoms. Electronegativity (χ), chemical potential (μ), global of hardness (η), global of softness (S), global of electrophilicity index (ω) and the absolute softness (σ) were evaluated according to definite equations[60,61]. One in-between important quantum parameters is the electrophilicity index (ω ,) which reflects the relative toxicity and reactivity of different selective sites. Whenever, electrophilicity may define the biological activity of proposed drugs. Also, indicates the stabilization energy while acquiring extra negative charge from the environment by drug systems. η and σ indicators, are measuring the molecular stability and reactivity. Also, their concepts are belonging to each others. The softness indicators are the vice verse character for global hardness [62].

3.8.2.1 quantum chemical parameters

The quantum parameters calculated are tabulated (Table 8) and the comparative investigation introduces the following notice; concerning free ligand. I) Soft character of the ligand expects its flexible reactivity towards the metal atoms. II) Positive electrophilicity indicator (χ) and negative electronic chemical potential (μ) values indicate that the compound is capable for capturing electrons from environment and its energy decrease coherently. Therefore, the electrochemical potential must be negative. While, the quantum parameters calculated for visualized structures are introducing the following important notice; I) The reduction of energy gapes (ΔE) in comparing with free ligand reflects the high softness of complexes and an expectation for distinguish biological activity. II) The reduction for E_{HOMO} than the free ligand may be accompanied with the strength of metallic bonds.III) The dipole moment values ordered by: Mn(II) > Co(II) > VO(II) > Ni(II) > HL > Cu(II). This order of arrangement agrees with the bigger the metal size the relatively ionic interaction bonds. This may clarify the interaction of donor ionic sites with Mn(II) and Co(II) ions than the others. This is considerably agrees with the spectral Racah parameter values estimated for Mn(II) and Co(II) complexes.

3.8.2.2. The bond lengths, atomic charges and oscillator strengths

According to numbering scheme and the data log file, essential bond lengths and effective charge density on coordinating sites were deducted and tabulated in Table 9. The chosen bonds relative to coordinating sites suffer an elongation than the genuine form of the ligand. This is supporting the mode of coordination. Also, the reduction of charges over O(10), N(6), N(7) and N(8) atoms in comparing with free ligand, verify their contribution in the mode. Whenever, the relatively reduced

charges over free N and O atoms, may refer to their participation in conjugation and presence of intra-ligand H-bonding. Oscillator strength is a quantity that indicates the permeability for the absorption or emission of radiation by the molecule consumed for transitions between energy levels. Its value can range from 0 to 1. A strong transition will have value close to 1. The calculated values reflect the relative lower electronic transition efficiency for such electronically condensed metal atoms.

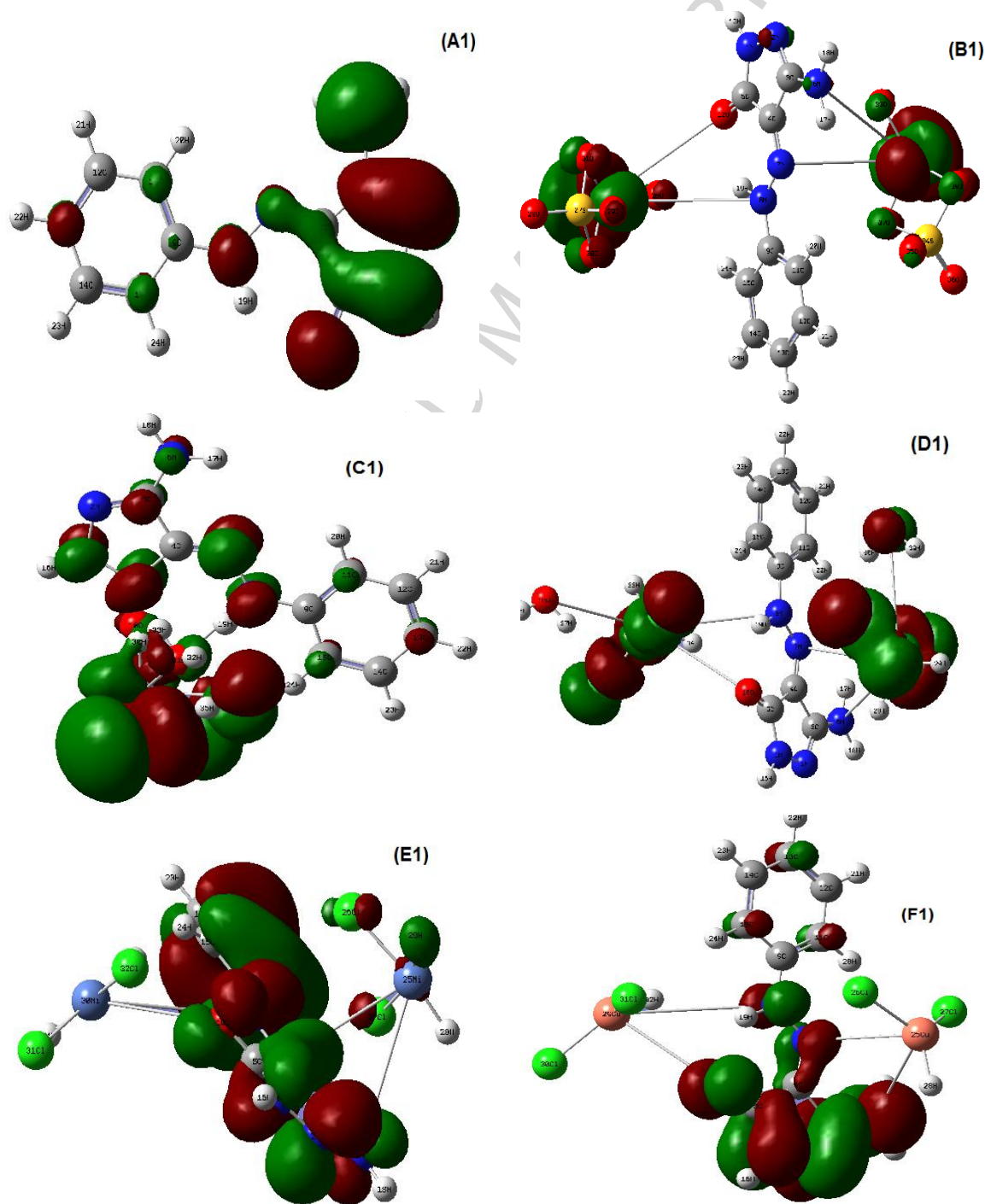


Fig. 4A. The frontier molecular orbital's of HOMO pictures for HL, VO(II), Mn(II), Co(II), Ni(II) and Cu(II) complexes(A,B,C,D,E and F, respectively)

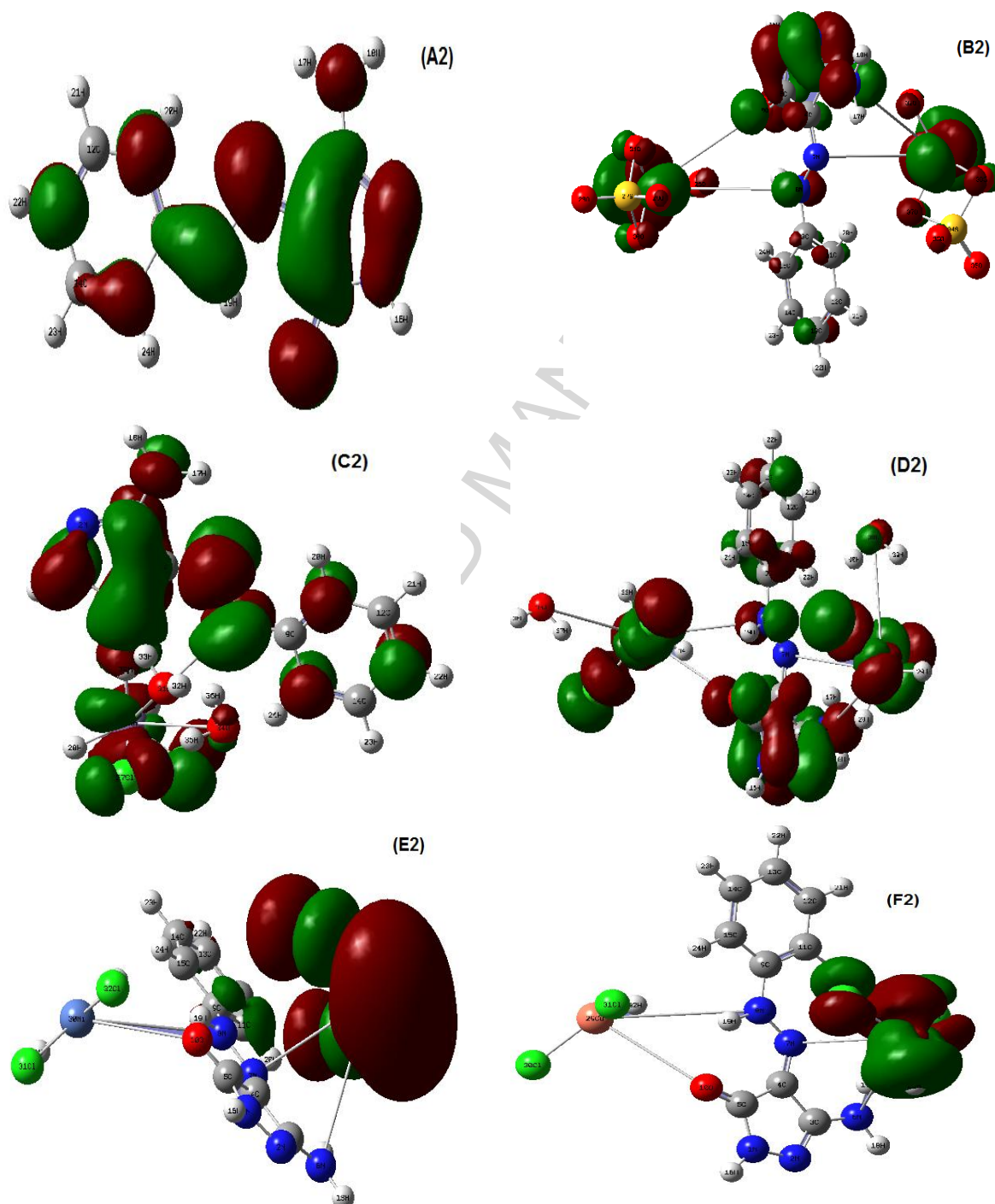


Fig.4B . The frontier molecular orbital's of LUMO pictures for HL, VO(II), Mn(II), Co(II), Ni(II) and Cu(II) complexes(A,B,C,D,E and F, respectively)

3.8.2.3 QSAR calculations

A interconnection between the anticancer activity of pyrazolone and its partition coefficient ($\log P=0.36$) is an inverse relationship[63]. A very low $\log P$ level reflects an expected distinguish activity. $\log P$ of the compound was determined for the optimized structures by HyperChem software. Whereby, the structure was slightly optimized by molecular mechanics force field (MM^+) and followed by precision adjustment with semi-empirical AM1. The structure optimized without confirming any indexes, leads to the geometry equilibrium state data (Table 10). The energy minimization protocol employed the Polake-Ribiere conjugated gradient algorithm.

3.8.3. Molecular docking

Recently, computer-encouraged drug design, different computational tools were enhanced dramatically by using more sophisticated and computationally intense methods. Autodock tools used to clarify the biological features of candidate drug or emphasis on experimental results. This study interested in using new designed drug to be used for antitumor investigation. The molecular docking was carried out for pyrazolone (Guest, fig 5) with different carcinoma protein receptors (Host) as: prostate carcinoma (2YXS, Crystal Structure of N-terminal domain of human galectin-8 with D-lactose, classification: sugar binding protein), colorectal carcinoma (2CGY, structure of helix pomatum agglutinin with Forssmann antigen) and hepatic carcinoma (2JW2, Validation of inter-helical orientation of the sterile-alpha-motif of human deleted in liver cancer 2 by residual dipolar couplings). The calculated energies for docking procedure are presented in Table 11. The binding free energy, constant of inhibition, energy of electrostatic, energy of total intercooled and receptor-inhibitor complexes interact surface were deduced. So, the reduction in binding energy due to mutation, will increase the inhibitor interaction affinity towards receptors [64]. The tabulated data display the best inhibition activity against 2YXS and 2JW2 protein receptors carcinoma. Also, reflect the best interaction stability for docked complexes (Fig. 6,6S). Accordance to computation, HB plot curves (Fig. 7,7S) clarify a high interaction with all receptors by comparable results. So, an expectation for its inhibition activity towards all tested carcinoma by excellent efficiency especially with prostate and liver cancers. This is referring to variable capability of multi-central groups for H-bonding interaction inside docking complexes. Inter-hydrogen bonding was appeared with all complexes excellently. 2D- plot curves (Fig. 8,8S) verify the mode of interaction inside the docking complex. Finally the anticancer efficiency of pyrazolone ligand will be substantially anticipated towards prostate and liver carcinoma cells.

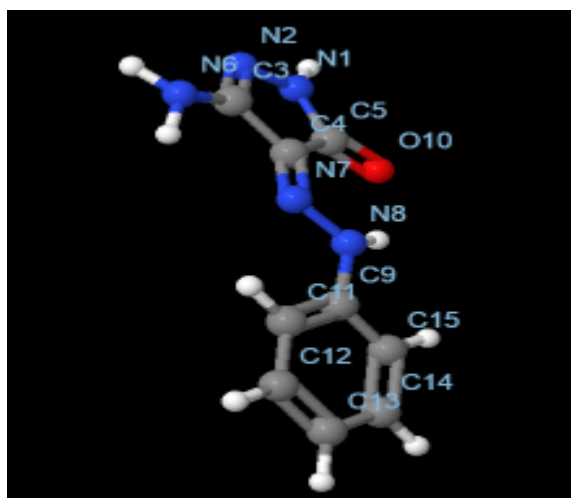


Fig. 5. The docked pyrazolone compound

3.9. Antitumor activity

Along the coordination chemistry a stationary increase of chemical products at various levels for different purposes. The coordination chemistry is considered one of most effective fields in anticancer drug design and development. Cancer, defines as uncontrolled cell division, and also characterized by dysregulation of apoptosis, proliferation, invasion, angiogenesis and metastasis [65]. Therefore, the expansion of drug scan prevents or keeps the aforementioned cancer properties under control considered a victory. In this study all the prepared complexes beside the original pyrazolone ligand were investigated towards HEPG2, PC3 and HCT116 cell lines in comparing with doxorubicin drug. HEPG2 cell viability and IC_{50} showed different responses depending on the complex. In comparing with doxorubicin referenced drug, the Cu(II) complex, displays the highest and significant effects towards hepatic and prostate carcinoma, while Mn(II) and VO(II) complexes display best impact towards colon and hepatic carcinoma cells, respectively. Contrary to expectations, Cu(II) complex, showed two folded impact than VO(II) complex, despite the known anticancer efficiency of VO(II) complexes in comparing with Cu(II) complexes. This may be due to the role of copper in regeneration of infected cell [66,67]. Likewise, the influence of Cu(II) complex presents linear effect, started with 0.01 doses which is seems as a small dose. Ni(II) complex was exhibited a significant impact also against HEPG2 (Table 12). While other elements present curved effect continued on a regular basis with the increase of the dose (Fig. 9). The ligand displays a very low influence on HepG2, while presented a high effect on both PC3 and HCT116. Co(II) complex exhibited different effect on different cell lines. While, HepG2 presented moderate response, PC3

displays very low response, but HCT116 was react more strongly. In the light of the outcomes, together with the results of previous in vivo and in vitro studies, suggest that the administration of Cu(II) complex may has a roll in prevention of liver and prostate cancers and [68]. PC-3 and HCT116 cell lines exhibit different response against the same complexes. Also, the main goal in our study is to introduce permissible complexes serve excellently as new designed drugs after other intensive examination from specialists. The complexes need further studies to investigate the pathway that may activate in different cancer cells. Here, the interaction mechanism may be discussed based on chelation theory [69]. On chelation, the charge of metal ion will be reduced by great magnitude due to the overlapping with donor orbital's. Further, over the whole chelate ring the increases in delocalization of p-electrons enhances the complex lipophilicity. The lipophilicity enhances the permeation into lipid membranes and closing the binding sites of infected cell enzymes.

4. Conclusion

The synthesized complexes using the pyrazolone ligand were investigated and characterized using all possible tools. The bi-nuclear complexes in the main feature except Mn(II) one. The spectral techniques have introduced the best molecular and structural formulas for the complexes. TG analysis and kinetic parameters are in importance to examine their thermal stability. Moreover, the theoretical investigation implementing different programs to emphasis on the experimental results may strengthen the study at all. As; Gaussian09 program optimizes the structural formulas applying DFT/B3LYP method. QSAR calculations expects the best inhibition of pyrazolone towards infected cells beside molecular docking outcomes. In comparing with referenced drug, IC_{50} calculated represented an excellent impact for Cu(II) complex in overcoming liver and prostate carcinoma, while the Mn(II) complex displays a high comparative impact against colon carcinoma cell line.

References

- [1] A. Gu'rsoy, M.S. Demirayak, G. C, apan, K. Erol, K. Vural, Eur. J. Med. Chem. 35 (2000) 359.
- [2] J.B. Jiang, D.P. Hesson, B.A. Dusak, D.L. Dexter, G.J. Kang, E. Hamel, J. Med. Chem. 33 (1990) 1721.
- [3] K. Anzai, M. Furuse, A. Yoshida, A. Matsuyama, T. Moritake, K. Tsuboi, N. Ikota, J. Radiat. Res. 45 (2004) 319.
- [4] E.A.M. Badawey, I.M. El-Ashmawey, Eur. J. Med. Chem. 33 (1998) 349.

- [5] G. Lemaire, W. Mnif, J.-M. Pascussi, A. Pillon, F. Rabenoelina, H. Fenet, E. Gomez C. Casellas, J.-C. Nicolas, V. Cavaillès, M.-J. Duchesne, P. Balaguer, *Tox. Sci.* **91** (2006) 501
- [6] C. B. Vicentini, D. Mares, A. Tartari, M. Manfrini, G. Forlani, *J. Agric. Food Chem.* **52** (2004) 1898
- [7] N. Singh, N. K. Sangwan, K. S. Dhindsa, *Pest. Manag. Sci.* **56** (2000) 284
- [8] B. Barszcz, *Coord. Chem. Rev.* **249** (2005) 2259
- [9] J. Bol, *Ph.D. Thesis*, University Leiden, Leiden, Netherlands, 1997
- [10] H. Sakurai, A. Tamura, J. Fugono, H. Yasui, T. Kiss, *Coord. Chem. Rev.* 245 (2003) 31–37 (and reference therein).
- [11] T.S. Smith, R. LoBrutto, V.L. Pecoraro, *Coord. Chem. Rev.* 228 (2002) 1–18.
- [12] D.M. Boghaei, S. Mohebi, *J. Mol. Catal. A: Chem.* 179 (2002) 41–51.
- [13] Khlood S. Abu-Melha, Nashwa M. El-Metwally, *Spectrochimica Acta Part A* 70 (2008) 277–283
- [14] Dubenko R. G.; Gorbenko E. F., *Chim. Geterocikl. Soedin.*, **1967**, 5, 923.
- [15] A.I. Vogel, *Text Book Of quantitative Inorganic Analysis* Longman, London (1986).
- [16] G.A. Bain, J.F. Berry, *Diamagnetic Corrections and Pascal's Constants*, *J. Chem. Educ.* 85(2008) 532.
- [17] E.S. Freeman, B. Carroll, *J. Phys.Chem.* 62 (1958)394-397.
- [18] W. Coats, *Kinetic Parameters from Thermogravimetric Data*, J.P. Redfern, *Nature*, 201(1964) 68
- [19] T. Ozawa, *A new method of analyzing thermogravimetric data*, *Bull. Chem. Soc. Japan.*, 38 (1965)1881-1886.
- [20] W.W. Wendlandt. *Thermal Methods of Analysis*, New York, Wiley (1974).
- [21] J.H.F. Flynn, L.A. Wall, *J. Res. Natl. Bur. Stand. A.*, 70 (1996)487.
- [22] P. Kofstad, *Oxidation of metals: Determination of activation energies*, *Nature.* 179 (1957)1362-1363
- [23] H.W. Horowitz, G.A. Metzger, *New analysis of thermogravimetric traces*, *Anal Chem.*, 35 (1963) 1464-1468 .
- [24] X. Wu. A.K. Ray, *Density-functional study of water adsorption on the PuO₂(110) surface* *Phys. Rev. B.*, 65, 85403 (2002).
- [25] M.J. Frisch, et al., *Gaussian 09, Revision D*, Gaussian, Inc., Wallingford, CT, 2010.
- [26] R. Dennington II, T. Keith, J. Millam, *GaussView, Version 4.1.2*, Semichem Inc, Shawnee Mission, KS, 2007.

- [27] T. A. Halgren *Journal of Computational Chemistry* 17 (5-6), 490-519 (1998)
- [28] G. M. Morris, D. S. Goodsell, et al. *Journal of Computational Chemistry* 19 (14), 1639-1662 (1998)
- [29] F. J. Solis and R. J. B. Wets "Minimization by Random Search Techniques *Mathematics of Operations Research* 6 (1), 19-30 (1981)
- [30] K. Nakamoto, P.J. McCarthy. *Spectroscopy and Structure of Metal chelate compounds*. John Wiley, New York, (1968).
- [31] U. El-Ayaan, M. M. Youssef, S. Al-Shihry, *J. Mol Struct.*, 936 (2009) 213-219.
- [32] R.K. Shah, K.S. Abou-Melha, F.A. Saad, T. Yousef, G.A.A. Al-Hazmi, M.G. Elghalban, A.M. Khedr, N.M. El-Metwaly., *J. Therm. Anal. Calorim.*, DOI 10.1007/s10973-015-4838-z, (2015)
- [33] A.A. Abou-Hussen, N.M. El-Metwaly, E.M. Saad, A.A. El-Asmy, *Coord. Chem.* 58 (2005) 1735.
- [34] M. B. Ferrari, S. Capacchi, G. Reffo, G. Aelosi, P. Tarasconi, R. Albertini, S. Pinellis, P. Lunghi, *J. of Inorg. Biochem.* 81(2000) 89.
- [35] C.K. Jorgensen, Fractional Charges, Integral Oxidation States and the Nephelauxetic Effect in the Five Transition Groups, *Helv. Chim. Acta.*, 50 (1967) 131-146.
- [36] Paola Deplano, Luca Pilia, Davide Espa, M. Laura Mercuri, Angela Serpe, *Coordination Chemistry Reviews* 254 (2010) 1434–1447
- [37] A. B. P. Lever, *Inorganic Electronic Spectroscopy*, Elsevier, Amsterdam, 1986
- [38] McGlynn SP, Smith JK. *J Mol Spectrosc.* 1961;6(188):198
- [39] R. T. Sanderson, *Inorganic Chemistry*, Chapter 6. Reinhold, New York (1967); H.J. Stoklosa. *J. Chem. Educ.*, 50, 50 (1973).
- [40] H.I. Park, L.J. Ming. *J. Inorg. Biochem.*, **27**, 57 (1998).
- [41] B.J. Hathaway, D.E. Billing. *Coord. Chem. Rev.*, **5**, 143 (1970); B.J. Hathaway, *Struct. Bonding (Berlin)*, **57**, 55 (1984).
- [42] H. Montgomery, E.C. Lingefetter. *Acta Cryst.*, **20**, 728 (1966).
- [43] D. Kivelson, R. Neiman. *J. Chem. Phys.*, **35**, **149** (1961)149.
- [44] R.C. Maurya, S. Rajput. *J. Molecular Structure*, **687**, 35 (2004).
- [45] J.A. Wellman, F.B. Hulsbergen. *J. Inorg. Nucl. Chem.*, **40**, 143(1978); U. Sagakuchi, A.W. Addison, *J. Chem. Soc. Dalton Trans.*, 660 (1979).
- [46] H. Yokoi, A.W. Addison, *Inorg. Chem.*, **16**, 1341 (1977).
- [47] R.K. Ray, G.R. Kauffman, *Inorg. Chem. Acta*, **173**, 207 (1990).
- [48] B. R. Mc Garvey, *J. Phys. Chem.* **71**, 51(1967).
- [49] R.C. Chikate, S.B. padhye, *Polyhedron*, **24**, 1689 (2005).

- [50] B.D. Cullity. Elements of X –ray diffraction. second ed., Addison –Wesley Inc., (1993).
- [51] A.A. Fahem, Spectrochim. Acta A, 88 (2012) 10-22.
- [52] A. Shahrjerdi, S. S. H. Davarani, E. Najafi, M. M. Amini, Ultrasonics Sonochemistry. 22 (2015) 382-390.
- [53] T. Yamanuchi, Y. Tsukahava, K. Yamada, T. Sakata, Y. Wada, Chem. Mater. **23** (2011) 75-84.
- [54] J.S. Ritch, T. Chivers, K. Ahmad, M. Afzaal, P.O. Brien., Inorg. Chem. 49, 1198 (2010); T. Mokari, M. Zhang, P. Yang, J. Am. Chem. Soc. 129 (2007) 9864-9865; J.J. Urban, D.V. Talapin, E.V. Shevchenko, C.B. Murray, J. Am. Chem. Soc., 128, (2006) 3248-3255.
- [55] B. Zhang, J. He, T.M. Tritt. Appl. Phys. Lett., 88, 043119 (2006); S.D. Robertson, T. Chivers. Dalton Trans.,1765 (2008).
- [56] Mukul Chauhan, Chemical Science Transactions, 2014, 3(4), 1455-1459
- [57] S.S. Kandil, G.B. El-Hefnawy, E.A. Baker, Thermal and spectral studies of 5-(phenylazo)-2-thiohydantoin and 5-(2-hydroxyphenylazo)-2-thiohydantoin complexes of cobalt (II), nickel (II) and copper (II) , Thermochim. Acta, 414 (2004) 105 -113.
- [58] Usama El-Ayaan, Nashwa M. El-Metwally, Magdy M. Youssef, Serry A.A. El Bialy, Spectrochimica Acta Part A 68 (2007) 1278–1286
- [59] I. Fleming, Frontier Orbitals and Organic Chemical Reactions, Wiley, London, 1976.
- [60] R.K. Ray, G.R. Kauffman, EPR spectra and covalency of bis(amidinourea/o-alkyl-1-amidinourea)copper (II) complexes. Part II. Properties of the CuN 42– chromophore, Inorg. Chem. Acta, 173 (1990) 207-214.
- [61] R.C. Chikate, S.B. padhye, Transition metal quinone-thiosemicarbazone complexes 2: Magnetism, ESR and redox behavior of iron (II), iron (III), cobalt (II) and copper (II) complexes of 2-thiosemicarbazido-1,4-naphthoquinone Polyhedron, 24 (2005) 1689 -1700.
- [62] S. Sagdinc, B. Köksoy, F. Kandemirli, S.H. Bayari, Theoretical and spectroscopic studies of 5-fluoro-isatin-3-(N-benzylthiosemicarbazone) and its zinc(II) complex J. Mol. Struct., **917**(2009) 63-70.
- [63] Riham F. George, European Journal of Medicinal Chemistry 47 (2012) 377-386
- [64] S. K. Tripathi , R. Muttineni , S. K. Singh, Journal of Theoretical Biology 334 (2013) 87–100
- [65] Al-Iede, M.M., J. Karpelowsky, and D.A. Fitzgerald. Recurrent diaphragmatic hernia: Modifiable and non-modifiable risk factors. Pediatr Pulmonol, (2015).
- [66] N. Terakado, S. Shintani, Y. Nakahara, *Oncol Rep*,**7**, (200) 1113-7.
- [67] C. Fosset, B. A. McGaw, M. D. Reid, *J Inorg Biochem*,**99**, (2005)1018-22.
- [68] C. Fosset, R. Danzeisen, L. Gambling, *J Inorg Biochem*,**103**, (2009) 709-16.

[69] S.H. Ataiw and A.A. Abou-Hussen, Egypt. J. Chem., 46, 685 (2003).

ACCEPTED MANUSCRIPT

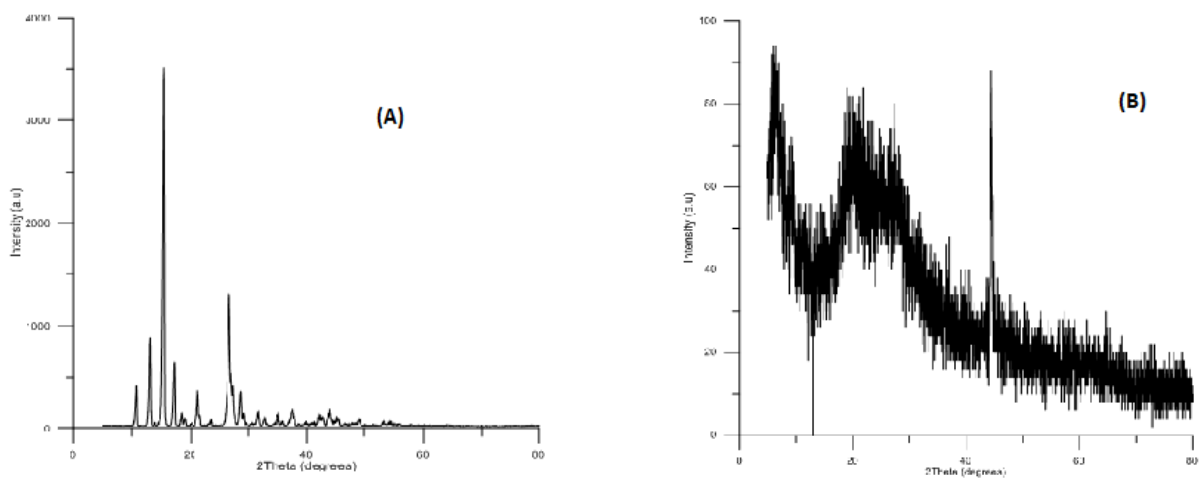


Fig. 3 . X-Ray manners of pyrazolone and VO(II) complex, A and B respectively

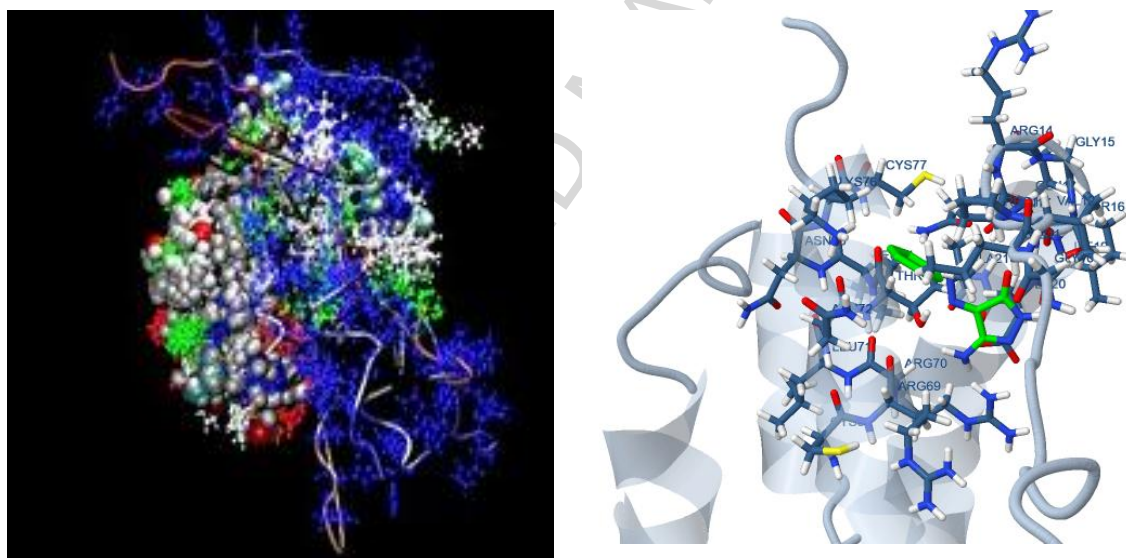


Fig. 5. Protein- inhibitor complex for 2JW2 receptor

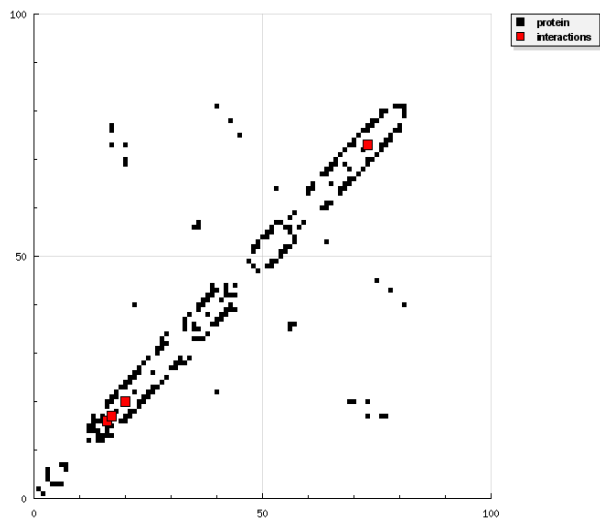
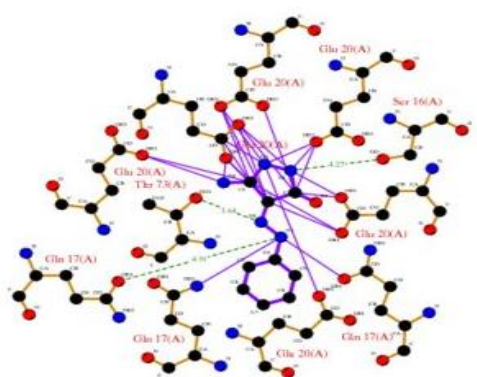


Fig. 6. HB plot of 2JW2 receptor with HL inhibitor



Key

- Ligand bond
- Non-ligand bond
- Hydrogen bond and its length
- Non-ligand residues involved in other contact(s)

docking

Fig. 7. 2D plot of 2JW2 receptor with HL inhibitor

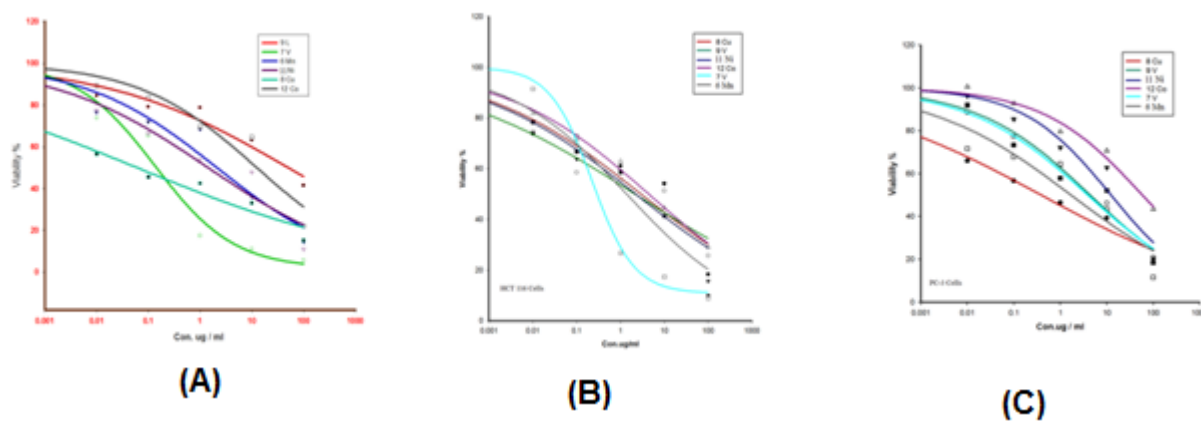


Fig. 8. Dose response curves against HEPG2, HCT116 and PC3, (A, B, C) respectively.

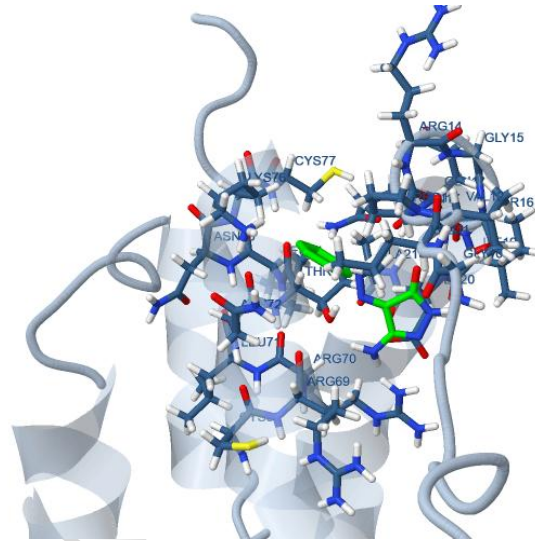
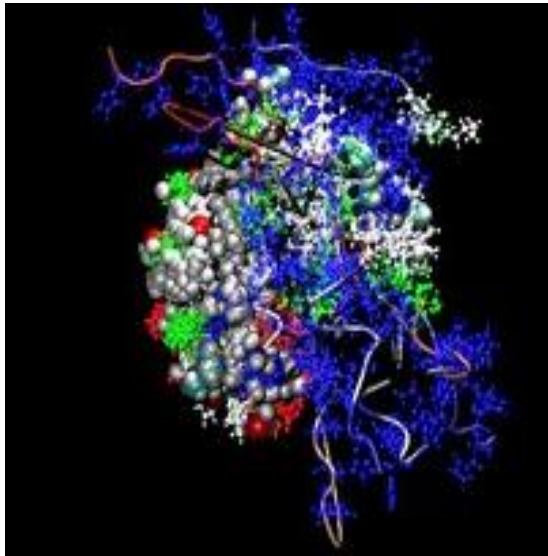


Fig. 6. Protein- inhibitor complex for 2JW2 receptor

Table 1. Analytical and physical data of pyrazolone ligand and its complexes.

Compound Empirical formula (Calcd)	Color	Elemental analysis (%) Calcd (Found)				
		C	H	N	Cl/SO ₄	M
1) [C ₉ H ₉ N ₅ O](203.204)	Deep orange	53.20(53.49)	4.46(4.34)	34.46(34.75)	----	----
2)[(VO) ₂ (SO ₄) ₂ (C ₉ H ₉ N ₅ O)]2H ₂ O(565.24)	Greenish-Brown	19.12(19.20)	2.32(2.31)	12.39(12.41)	33.99(34.11)	18.03(18.00)
3)[MnCl ₂ (C ₉ H ₉ N ₅ O).2(H ₂ O)](365.08)	Orange	29.61(29.56)	3.59(3.60)	19.18(19.20)	9.71(9.71)	15.05(15.10)
4)[Co ₂ Cl ₄ (C ₉ H ₉ N ₅ O).4(H ₂ O)](534.94)	Dark-Brown	20.21(20.16)	3.20(3.20)	13.09(13.11)	26.51(26.49)	22.03(22.02)
5)[Ni ₂ Cl ₄ (C ₉ H ₉ N ₅ O)]2H ₂ O(498.43)	Pale-Brown	21.69(21.70)	2.63(2.60)	14.05(13.98)	12.02(12.10)	23.55(23.53)
6)[Cu ₂ Cl ₄ (C ₉ H ₉ N ₅ O)]2H ₂ O(508.14)	Pale-Brown	21.27(21.26)	2.58(2.57)	13.78(13.80)	11.98(11.97)	25.01(25.11)

Table 2. Significant IR spectral bands (cm⁻¹) of pyrazolone ligand and its complexes

Compound	$\nu_{\text{NH}_2+\text{VOH}}$	ν_{NH}	$\nu_{\text{C=O}}$	$\nu_{\text{C=N}}$	δ_{NH_2}	δ_{NH_s}	$\frac{\delta_{\text{r}}(\text{H}_2\text{O})}{\delta_{\text{w}}(\text{H}_2\text{O})}$	VM-O	VM-N
1) [C ₉ H ₉ N ₅ O]	3410,3333	3185	1671	1586	1625	1442,1493	---	----	----
2)[(VO) ₂ (SO ₄) ₂ (C ₉ H ₉ N ₅ O)]2H ₂ O	3398	3173	1652	1551	1595	1437,1485	875,662	592	490
3)[MnCl ₂ (C ₉ H ₉ N ₅ O).2(H ₂ O)]	3336,3352	3165	1683	1597	1637	1439,1496	781,683	461	449
4)[Co ₂ Cl ₄ (C ₉ H ₉ N ₅ O).4(H ₂ O)]	3320,3331	3160	1650	1552	1600	1436,1473	860,668	586	527
5)[Ni ₂ Cl ₄ (C ₉ H ₉ N ₅ O)]2H ₂ O	3331(center)	----	1640	1559	1590	1432,1498	860,668	533	490
6)[Cu ₂ Cl ₄ (C ₉ H ₉ N ₅ O)]2H ₂ O	3443, 3309	3177	1682	1574	1597	1366,1496	880,684	575	467

Table 3. Spectroscopic , covalence parameters and magnetic moment values

Compound	$\nu_1(\text{cm}^{-1}), \nu_2$	ϵ_1, ϵ_2	$(\times 10^{-5}) f_1$ f_2	Intraligand and charge transfer(cm ⁻¹)	Z	μ_{eff} (BM)
----------	--------------------------------	--------------------------	---------------------------------	--	---	----------------------------

1)	23,809	454	2150	31,250;25,000	----	-----
2)	13,150	364	130	31,158; 26,521	+1.49 8	1.34
3)	18,420	25	32	31,250;27,027; 23,529		5.96
4)	16,255;19,560	320;18 9	195;15 5	30,303; 25,000	+1.43 6	4.31
5)	19,450	120	199	30,303; 20,833		0.00
6)	18,590	295	18	31,250;25,400;20,00 0		1.46

* Molar absorptivity, ** Oscillator strengths, f , calculated using the following expression: $f = 4.6 \times 10^{-9} \epsilon_{\max} \nu_{1/2}$, where; ϵ_{\max} is the molar absorptivity of the band maximum and $\nu_{1/2}$ is the band width at half-height expressed in wave numbers :C. J. Ballhausen, Prog. Inorg. Chem. 2.251(1960)

Table 4. Spin – Hamiltonian parameters of VO(II) and Cu(II) complexes (A and p $\times 10^4$)

Complex	g_{11}	g_{\perp}	g_o	A_{11}	f	A_{\perp}	A_o	p	k	${}^2K_{//}$	${}^2K_{\perp}$	α^2	β^2
2)	1.935	1.992	1.97	169.3	114.2	67.7	101.6	118.2	0.829	-1.010	-0.640	0.568	0.933
			3		7		0	8					
6)	2.336	2.185	2.23	176.3	132.4	66.26	102.9	219.4	0.702	-0.934	-2.045	0.934	0.994
			5		5		5	5					

Table 5. XRD spectral data of pyrazolone ligand and its nano-crystalline complexes

Compound	Size (Å)	2 θ	Intensity	d-spacing(Å)	FWHM
1)	2.782	17	3500	5.211	0.5263
3)	3.473	16	219.4	5.535	0.4211
6)	2.723	15	455.2	5.901	0.5364

Table 6. Assumed TG analysis data for investigated compounds

Complex	Steps	Temp. range(°C)	Decomposed	Weight loss; Calcd (Found %)
(1)	1 st	50.11 - 180.23	-[NH ₂ CN]	20.69(20.56)
	2 nd	180.24 - 502.31	-[C ₆ H ₄ N ₂]	52.22(52.32)
	3 rd	502.31 - 803.12	-[HCNO]	21.17(21.03)
	Residue		C	5.91(6.09)
(2)	1 st	51.43 – 310.22	-[2H ₂ O+2SO ₃ +O ₂]	40.36(40.41)
	2 nd	310.22 – 622.12	-[C ₉ H ₉ N ₅ O]	35.95(36.02)
	Residue		V ₂ O ₂	23.68(23.57)
(3)	1 st	51.02 – 185.28	-[2H ₂ O+Cl ₂]	29.29(29.31)
	2 nd	185.28 – 622.76	-[C ₉ H ₉ N ₅]	51.28(51.10)
	Residue		MnO	19.43(19.59)

(4)	1 st	150.21 – 421.78	-[2H ₂ O+2Cl ₂ +N ₂]	45.22(45.11)
	2 nd	421.78 – 826.34	-[C ₉ H ₉ N ₃]	29.76(29.68)
	Residue		CoO+Co	25.02(25.21)
(5)	1 st	56.20 – 178.71	-[2H ₂ O+Cl ₂]	21.45(21.42)
	2 nd	178.71 – 448.51	-[Cl ₂ + C ₆ H ₆ +N ₂]	35.52(35.54)
	3 rd	448.51 – 815.61	-[C ₃ H ₃ N ₃ O]	19.48(19.48)
	Residue		2Ni	23.55(23.56)
(6)	1 st	32.20 – 351.43	-[2H ₂ O+2Cl ₂]	34.99(35.02)
	2 nd	351.43 – 825.90	-[C ₉ H ₉ N ₅]	36.84(36.72)
	Residue		CuO+Cu	28.16(28.26)

Table 7. Coats–Red fern (CR) and Horowitz–Metzger (HM) kinetic parameters

Comp.	Step	Method	Kinetic Parameters					
			E (Jmol ⁻¹)	A (S ⁻¹)	Δ S(Jmol ⁻¹ K ⁻¹)	Δ H (Jmol ⁻¹)	Δ G (Jmol ⁻¹)	r
1)	2 nd	CR	1.02E+05	1.81E+06	-1.31E+02	9.64E+04	1.78E+05	0.9993
		HM	1.07E+05	1.00E+07	-1.17E+02	1.02E+05	1.75E+05	0.9991
2)	2 nd	CR	6.43E+04	1.21E+02	-2.13E+02	5.80E+04	2.18E+05	0.9993
		HM	7.93E+04	1.33E+03	-1.93E+02	7.31E+04	2.18E+05	0.9991
3)	2 nd	CR	1.36E+05	1.18E+09	-7.74E+01	1.31E+05	1.79E+05	0.9993
		HM	1.40E+05	5.31E+09	-6.49E+01	1.34E+05	1.75E+05	0.9991
4)	1 st	CR	4.71E+04	2.72E+01	-2.23E+02	4.20E+04	1.78E+05	0.9993
		HM	5.66E+04	3.30E+02	-2.03E+02	5.15E+04	1.75E+05	0.9991
5)	2 nd	CR	4.55E+04	7.88E+00	-2.33E+02	4.06E+04	1.79E+05	0.9993
		HM	5.64E+04	4.62E+02	-2.00E+02	5.15E+04	1.70E+05	0.9991
6)	1 st	CR	8.23E+04	1.59E+05	-1.51E+02	7.77E+04	1.61E+05	0.9993
		HM	9.39E+04	6.15E+06	-1.20E+02	8.93E+04	1.56E+05	0.9991

Table 8. The DFT/B3LYP parameters calculated for optimized structures

Compound	E _H (eV)	E _L (eV)	(E _H - E _L) (eV)	E _r -E _h	x(eV)	μ(eV)	η(eV)	S(eV-1)	ω(eV)	σ(eV)
Li	-0.19678	-0.08087	-0.1159	0.11591	0.138825	-0.13883	0.057955	0.028978	0.16627	17.25476663
VO(II)	-0.21198	-0.19919	-0.0128	0.01279	0.205585	-0.20559	0.006395	0.003198	3.30455	156.3721658
Mn(II)	-0.18647	-0.14986	-0.0366	0.03661	0.168165	-0.16817	0.018305	0.009153	0.772452	54.62988255
Co(II)	-0.23844	-0.22224	-0.0162	0.0162	0.23034	-0.23034	0.0081	0.00405	3.275094	123.4567901

Ni(II)	-0.29905	-0.15049	-0.1486	0.14856	0.22477	-0.22477	0.07428	0.03714	0.340075	13.46257404
Cu(II)	-0.11332	-0.0719	-0.0414	0.04142	0.09261	-0.09261	0.02071	0.010355	0.207065	48.28585225

Table 9. Significant bond lengths, charges, dipole moment(D), oscillator strength(f)and excitation energies(E)

Compound	O ¹⁰ N ⁶	N ⁷ N ⁸	⁵ C=O ¹⁰	³ C-N ⁶	⁴ C=N ⁷	⁹ C-N ⁸	M ₁ M ₂	D(Debye)	f	E(nm)
1)	-0.448387 -0.111306	-0.205846 -0.270725	1.22095 6	1.370781	1.29019 2	1.40422 3	----	2.9244	0.0341	483.09
2)	-0.474897 -0.088761	-0.350330 -0.226567	1.23930 8	1.370490	1.29560 9	1.40551 4	0.951900 0.944626	5.9680	0.0017	12361.8
3)	0.223956 -0.648275	-0.058359 -0.428142	1.22107 8	1.371431	1.28964 7	1.40333 0	-0.585802	12.427 7	0.0004	4431.92
4)	-0.447236 -0.070013	-0.341460 -0.191357	1.23341 8	1.370473	1.29420 8	1.40422 5	0.276905 0.280089	6.0396	0.0016	6456.08
5)	-0.439258 -0.072732	0.066487 -0.215595	1.23231 1	1.370616	1.29351 0	1.40527 4	0.280117 0.217763	4.2849	0.0021	4539.19
6)	-0.242813 0.072489	-0.136675 0.042351	1.23242 7	1.370590	1.29359 7	1.40531 3	0.457526 0.439187	2.3612	0.0001	4202.59

Table 10. QSAR calculations for fully optimized pyrazolone compound

Total Energy	-60609.4872650 (kcal/mol)	Surface area	303.14Å
Total Energy	-96.587354109 (a.u.)	Surface area (Grid)	394.39 Å
Binding Energy	-2540.7823370 (kcal/mol)	Volume	611.19 Å
Isolated Atomic Energy	-58068.7049280 (kcal/mol)	Hydration energy	- 16.49 Kcal/mol
Electronic Energy	-320832.6521163 (kcal/mol)	Log P	0.36
Core-Core Interaction	260223.1648512 (kcal/mol)	Reactivity	58.85 Å
Heat of Formation Gradient	90.7046630 (kcal/mol) 0.0984258 (kcal/mol/Ang)	Polar ability Mass	21.17 Å 203.2amu

Table 11. Molecular docking energy values for pyrazolone - protein receptors complexes

receptor	Est. free energy of binding (kCal/mol)	Est. inhibition constant (K _i)(uM)	vdW+ bond+ desolve energy (kCal/mol)	Electrostatic Energy (kCal/mol)	Total intercooled Energy (kCal/mol)	Frequency	Interact surface
2YXS	-4.50	505.06	-4.53	-0.47	-4.99	30%	400.077
2CGY	-3.78	1.68	-4.06	-0.20	-4.26	20%	396.394
2JW2	-4.47	527.01	-4.47	-0.61	-5.08	40%	421.434

Table 12. The impact of investigated compounds against HEPG2, PC3 and HCT116 cell lines.

Cell type	IC ₅₀ (µg/ml)					
	L	VO	Mn	Ni	Co	Cu Doxorubicin
HEPG2	50.87	0.13	2.13	1.43	12.57	0.061 0.777
PC3	4.376	3.8895	1.701	12.3	58.3837	0.389 0.9255
HCT116	2.155	1.38	0.2213	2.223	4.4211	2.96 0.8105

ACCEPTED MANUSCRIPT

Highlights

- 1- A series of VO(II), Mn(II), Co(II), Ni(II) and Cu(II) - pyrazolone complexes were synthesized and characterized
- 2- Thermal analysis and kinetic parameters are concerned in study to examine the thermal stability of complexes
- 3- Using Gaussian09 program to optimize the structural formula for the investigated compounds
- 4- QSAR calculations proposes a distinguish biological activity for pyrazolone ligand

ACCEPTED MANUSCRIPT